Received: 13 November 2019 | Revised: 3 February 2020 | Accepted: 4 February 2020

DOI: 10.1111/mmi.14483

WILEY

RESEARCH ARTICLE

A novel septal protein of multicellular heterocystous cyanobacteria is associated with the divisome

Benjamin L. Springstein [1] | Sergio Arévalo [2] | Andreas O. Helbig [3] | Antonia Herrero [2] | Karina Stucken [4] | Enrique Flores [2] | Tal Dagan [1]

[1]Institute of General Microbiology, Christian-Albrechts-Universität zu Kiel, Kiel, Germany

[2]Instituto de Bioquímica Vegetal y Fotosíntesis, CSIC and Universidad de Sevilla, Seville, Spain

[3]AG Proteomics & Bioanalytics, Institute for Experimental Medicine, Christian-Albrechts-Universität zu Kiel, Kiel, Germany

[4]Department of Food Engineering, Universidad de La Serena, La Serena, Chile

Correspondence
Benjamin L. Springstein, Institute of General Microbiology, Christian-Albrechts-Universität zu Kiel, Kiel, Germany.
Email: benjamin_springstein@hms.harvard.edu

Present address
Benjamin L. Springstein, Department of Microbiology, Blavatnick Institute, Harvard Medical School, Boston, MA, USA

Funding information
Deutsche Forschungsgemeinschaft, Grant/Award Number: STU513/2-1; Spanish Government and European Regional Development Grant, Grant/Award Number: BFU2016-77097-P and BFU2017-88202-P

Abstract

Cyanobacteria are unique among the eubacteria as they possess a hybrid Gram phenotype, having an outer membrane but also a comparably thick peptidoglycan sheet. Furthermore, the cyanobacterial divisome includes proteins specific for both the Gram types as well as cyanobacteria-specific proteins. Cells in multicellular cyanobacteria share a continuous periplasm and their cytoplasms are connected by septal junctions that enable communication between cells in the filament. The localization of septal junction proteins depends on interaction with the divisome, however additional yet unknown proteins may be involved in this process. Here, we characterized Alr3364 (termed SepI), a novel septal protein that interacts with the divisome in the multicellular heterocystous cyanobacterium *Anabaena* sp. strain PCC 7120. SepI localized to the Z-ring and the intercellular septa but did not interact with FtsZ. Instead, SepI interacted with the divisome proteins ZipN, SepF and FtsI and with the septal protein SepJ. The inactivation of *sepI* led to a defect in cell filament integrity, colony and cell morphology, septum size, nanopore formation and peptidoglycan biogenesis, and inability to differentiate heterocysts. Our results show that SepI plays a role in intercellular communication and furthermore indicate that SepI functions in the coordination of septal junction localization during cell division.

1 | INTRODUCTION

Cyanobacteria are a monophyletic group that includes species having diverse morphologies, ranging from unicellular species to filamentous and cell-differentiating strains (Garcia-Pichel, Zehr, Bhattacharya, & Pakrasi, 2020; Rippka, Stanier, Deruelles, Herdman, & Waterbury, 1979). The major characteristics of prokaryotic multicellularity are the manifestation of cell-cell attachment sites, mechanisms of cell-cell communication (e.g., through junctional complexes) and a division of labor among cells in the colony (Claessen, Rozen, Kuipers, Søgaard-Andersen, & Wezel, 2014; Flores, Herrero, Forchhammer, & Maldener, 2016). The filamentous cyanobacterium *Anabaena* sp. strain PCC 7120 (hereafter *Anabaena*) reproduces through random trichome (i.e., filament) breakage and grows by intercalary cell division; the multicellular phenotype of *Anabaena* is maintained through incomplete segregation of cells following division (Claessen et al., 2014; Rippka et al., 1979). Individual cells within an *Anabaena* filament possess an individual cytoplasmic

membrane and peptidoglycan (PG) sheets, yet, all cells are engulfed in a continuous outer membrane and hence are connected by a shared periplasm (Wilk et al., 2011). In the absence of combined nitrogen, *Anabaena* produces heterocysts, which are specialized cells where atmospheric nitrogen is fixed into a bioavailable nitrogen form (ammonia). Heterocyst differentiation includes an inhibition of oxygenic photosynthesis, hence they supply a micro-aerobic environment that increases the efficiency of nitrogen fixation (Kumar, Mella-Herrera, & Golden, 2010). As a result of this cell specialization, a metabolic communication between heterocysts and vegetative cells in the *Anabaena* filament is essential to exchange photosynthates and combined nitrogen products between the two cell types (Herrero, Stavans, & Flores, 2016). Thus, the unique characteristics of cyanobacterial multicellularity hinge upon mechanisms for inter-cellular communication.

The communication among cells in the *Anabaena* filament is supported by cell-cell joining structures that are termed "septal junctions" and are analogous to the eukaryotic gap junctions (Flores et al., 2016; Wilk et al., 2011). The *Anabaena* septal junctions are putatively composed of several proteins, among which are SepJ, FraC and FraD, whose deletion abrogated intercellular molecular exchange, hence they were considered putative septal junction components (Flores et al., 2007; Merino-Puerto, Mariscal, Mullineaux, Herrero, & Flores, 2010; Mullineaux et al., 2008; Nürnberg et al., 2015). The role of FraD in septal junctions recently gained additional support with the observation of septal junction structures that link the cytoplasms of neighboring cells and contain FraD (Weiss, Kieninger, Maldener, Forchhammer, & Pilhofer, 2019). Septal junctions mediate molecular diffusion between adjacent cells and are likely regulated by gating, thus predating the gated mechanism of eukaryotic gap junctions (Flores, Nieves-Morión, & Mullineaux, 2018; Nieves-Morión, Mullineaux, & Flores, 2017; Nürnberg et al., 2015; Weiss et al., 2019). The *Anabaena* septal junctions traverse the septal PG through holes, termed "nanopores", whose formation is dependent on PG amidases (AmiC) and the PG binding protein SjcF1 (Bornikoel et al., 2017; Rudolf et al., 2015). The inactivation of *sepJ*, *fraC* and *fraD* is associated with filament fragmentation mainly under diazotrophic conditions, indicating a function of these proteins in filament integrity (Merino-Puerto et al., 2010; Nayar, Yamaura, Rajagopalan, Risser, & Callahan, 2007). Furthermore, heterocyst-formation is strictly dependent on the SepJ function but not on FraC and FraD (Flores et al., 2007; Merino-Puerto et al., 2010). SepJ is thought to interact with the PG sheet by means of its coiled-coil (CC) domain. Furthermore, SepJ forms multimers, hence it might form a structure that is reminiscent of the gap junctions buildup, which consist of two connexin hexamers (Ramos-León, Mariscal, Battchikova, Aro, & Flores, 2017). The localization of SepJ to the septa in *Anabaena* is dependent on its interaction with the divisome during cell division, nonetheless no direct interaction was found between SepJ and FtsZ (Ramos-León, Mariscal, Frías, Flores, & Herrero, 2015).

Cell division in bacteria is governed by the divisome, a multi-protein complex that is formed at the future division site upon polymerization of FtsZ (the prokaryotic tubulin homolog), which assembles into the Z-ring below the cytoplasmic membrane. FtsZ is tethered to the cytoplasmic membrane by an interaction with proteins such as FtsA and ZipA that are linked to the cytoplasmic membrane through an amphipathic helix (FtsA) or a transmembrane helix (ZipA). The divisome governs chromosome segregation and PG remodeling as well as septum invagination and ultimately cell septation (den Blaauwen, Hamoen, & Levin, 2017). In *Anabaena*, FtsZ is an essential cellular component that includes an N-terminal peptide specific to filamentous heterocystous cyanobacteria (Corrales-Guerrero et al., 2018; Zhang, Hugenin, Friry, Huguenin, & Friry, 1995). Additionally, several other components of the *Anabaena* divisome have been identified, including FtsK, FtsW, FtsQ and FtsI. Although generally characterized as Gram-negative bacteria, cyanobacteria possess conserved Gram-positive bacteria-specific cell division proteins such as DivIVA (also known as Cdv3) and SepF, suggesting that a clear Gram classification is not applicable for that phylum (MacCready, Schossau, Osteryoung, & Ducat, 2017; Marbouty, Saguez, Cassier-Chauvat, & Chauvat, 2009; Miyagishima, Wolk, & Osteryoung, 2005). Furthermore, cyanobacteria lack the FtsZ membrane tethering proteins FtsA and ZipA and possess cyanobacterial-specific cell division proteins such as ZipN (also known as Ftn2) and Ftn6 (Koksharova & Wolk, 2002; Marbouty, Mazouni, Saguez, Cassier-Chauvat, & Chauvat, 2009; Marbouty, Saguez, et al., 2009; Miyagishima et al., 2005). The *Anabaena* ZipN was found to recruit FtsZ to the cytoplasmic membrane and interact with a wide array of divisome proteins, including Ftn6, SepF, FtsW, FtsX, FtsQ and FtsI (Camargo et al., 2019). ZipN also interacts with SepJ and regulates its septal localization. As such, ZipN links cell division-related processes to septum formation, intercellular communication and filament integrity (Camargo et al., 2019).

In this work, we aimed to identify additional proteins that play a role in the coordinated process of cell division and the formation of septal junctions. Our results identified a novel coiled-coil-rich protein (CCRP) in *Anabaena* that is localized in the septum, interacts with the divisome, and has a putative role in filamentation.

2 | RESULTS

2.1 | SepI is ubiquitous in filamentous heterocyst-forming cyanobacteria

A survey for proteins containing a high coiled-coil content (using COILS) and hence a putative function in *Anabaena* multicellularity revealed the gene *alr3364* (termed here *sepI*), which includes two N-terminal coiled-coil domains and a FtsK-like domain at the C-terminus (Figure 1a). Notably, SepI shows resemblance to parts of SepJ (Supplementary Figure S1). In addition to the two N-terminal coiled-coils, the C-terminal non-coiled-coil domain of SepI (from aa 241 on) has a similar amino acid composition to the linker domain of SepJ (Herrero et al., 2016) and is also rich in proline (15%), serine (11%) and threonine (8%), suggesting similar involvements in cellular

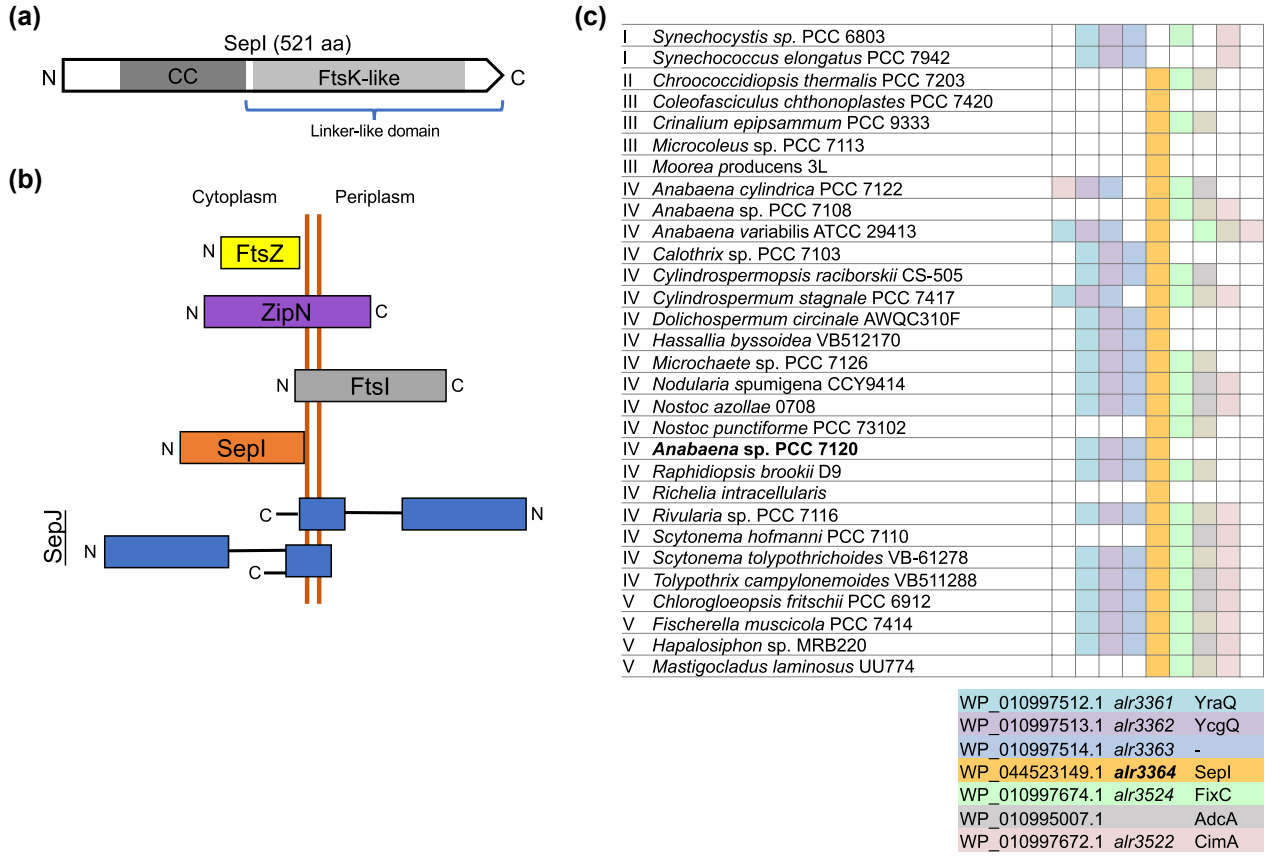

FIGURE 1 Domain architecture, predicted localization and conservation of SepI. (a) Schematic depiction of the domain architecture of SepI. The CC domain, the FtsK-like domain and the domain similar to the linker domain of SepJ are indicated. (b) Schematic depiction of subcellular localization of selected divisome and septal junction proteins from *Anabaena*. Localization of FtsZ, ZipN and FtsI is inferred from (Camargo et al., 2019). N indicates the N-terminus and C indicates the C-terminus of the respective protein. For practical reasons, indication of the C-terminus for FtsZ and SepI was omitted. Close localization of SepI to the cytoplasmic membrane indicates a likely interaction with the cytoplasmic membrane. The precise localization of SepJ is still under debate with the N-terminal CC and linker domain localized in the periplasm or cytoplasm (Ramos-León et al., 2017, 2015). (c) Gene order in the neighborhood of genes encoding SepI homologs in cyanobacterial genomes. Note that *alr3361*, *alr3362*, and *alr3363* have homologs in all cyanobacteria genomes tested with only few exceptions (i.e., they are universal). Homologs of *alr3524* and *alr3522* are abundant in all organisms (see full lists and accession numbers in Supplementary File 1). Organisms are marked according to their morphological phenotype: I, unicellular cyanobacteria that divide by binary fission; II, unicellular organisms that can divide in multiple planes; III, filamentous; IV, filamentous and heterocyst forming; V, heterocyst forming and true branching or multiseriate filaments

processes of both, the C-terminal SepI domain and the linker domain of SepJ. Unlike SepJ, which is a polytopic multipass transmembrane (TM) protein (Figure 1b), we found no evidence for TM domains in the SepI sequence (predicted with TMHMM). A computational prediction of SepI localization suggested that it is localized in the cytoplasm (predicted using PSORTb) and interacts with the cytoplasmic membrane through its C-terminus (predicted using Gneg-mPLoc and PSIPRED). The lack of a signal peptide and of an amphipathic helix in SepI (as predicted using SignalP-5.0 and AmphipaSeek respectively) are also consistent with a putative cytoplasmic localization (Figure 1b).

A survey for homologs to *sepI* in cyanobacterial genomes showed that *sepI* is ubiquitous in heterocystous cyanobacteria and *sepI* homologs are rarely found in non-heterocystous species (Figure 1c, Supplementary File 1). Notably, none of the investigated cyanobacterial genomes of subsection I contained a *sepI* homolog (Supplementary File 1). Furthermore, the genomic neighborhood of *sepI* homologs, including the upstream genes *alr3361*, *alr3362* and *alr3363*, is highly conserved in heterocystous cyanobacteria (Figure 1c; Supplementary File 1). Although these genes could form an operon together with *sepI*, a specific transcription start-site has been previously identified for *sepI* (Mitschke, Vioque, Haas, Hess, & Muro-Pastor, 2011). Downstream of *sepI*, ORFs *alr3365* and *alr3366* are located in the same orientation. Nonetheless, RT-PCR tests did not support the occurrence of common transcripts (Supplementary Figure S2a,b).

2.2 | SepI localizes to the mid-cell and the septa

To investigate the intracellular localization of SepI, we expressed a SepI-GFP fusion (in which the GFP was added to the C-terminus of SepI) from the predicted native promoter (P_{sepI}, encompassing

602 bp upstream of *sepI*; see Supplementary Figure S2a). Additionally, to observe the putative effects from protein overexpression, we also expressed SepI-GFP from the comparably strong copper-inducible P_{petE} promoter. Both constructs were carried on plasmid pRL25C. Regardless of the promoter, SepI-GFP localized to the mid-cell in ring forms reminiscent of the Z-ring and to the septa between neighboring cells (Figure 2a). Notably, the septal localization of SepI-GFP between the vegetative cells and heterocysts seemed to be restricted to the vegetative cell side as it was never observed at the heterocyst side (zoom-in in Figure 2a). Further examination of 150 samples of SepI-GFP localization in the neighborhood of heterocysts showed that none of the samples contained apparent septal SepI-GFP signals at the heterocysts side (this is unlike what we have observed for example for SepJ-YFP, which shows clear localization at the heterocyst-side; see also the localization of SepJ-GFP in Flores et al., 2007). We are aware, however, that the limited resolution of epifluorescence microscopy is likely not sufficient in order to fully discard the presence of SepI in the heterocysts.

2.3 | SepI is involved in filament integrity as well as cell and colony morphology

To further elucidate the functional role of SepI in *Anabaena*, we generated a Δ*sepI*::C.S3 mutant strain (Supplementary Figure S2c). We obtained two independent fully segregated mutant strains, both showing the same phenotypic properties. We also verified by semi-quantitative RT-PCR that the genomically inserted C.S3 cassette (Elhai & Wolk, 1988) did not affect the expression of the

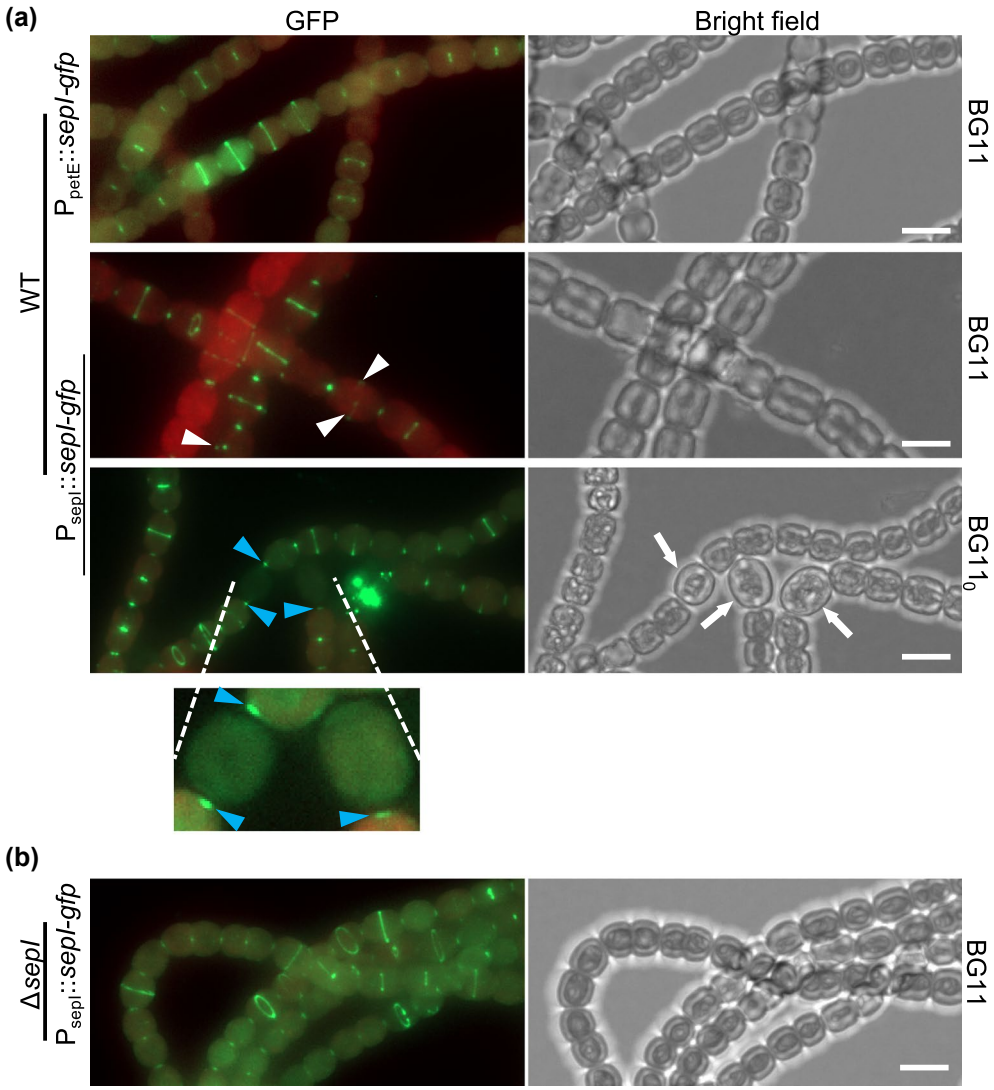

FIGURE 2 SepI is associated with the Z-ring and the septa. Merged GFP fluorescence and chlorophyll autofluorescence (red) and bright field micrographs of (a) *Anabaena* WT or (b) Δ*sepI*::C.S3 mutant cells expressing SepI-GFP from P_{sepI} or P_{petE} promoters. Cells were either grown on BG11 or $BG11_0$ plates. White triangles indicate Z-ring formation that simultaneously nucleated from more than one site. Blue triangles highlight the SepI-GFP localization between vegetative cells and heterocysts, which seems restricted to the vegetative cell. White arrows indicate heterocysts. Scale bars: 5 μm

downstream genes *alr3365* and *alr3366* (Supplementary Figure S2b). In the presence of nitrate, the Δ*sepI* mutant showed no detectable growth defect in liquid culture in comparison to the wild-type strain (Supplementary Figure S2d). However, the Δ*sepI* mutant was unable to grow diazotrophically (i.e., on $BG11_0$ plates or in $BG11_0$ liquid medium; Figure 3e, Supplementary Figure S2e). Strain Δ*sepI* readily fragmented when incubated in $BG11_0$ medium (Figure 3a,b), suggesting a function of SepI in filament integrity. Notably, we observed that the Δ*sepI* mutant never differentiated heterocysts. Additionally, the Δ*sepI* mutant was characterized by an abnormal cell shape and colony morphology under standard growth conditions (i.e., in BG11 liquid or on BG11 plates; Figure 3c), with an increase in cell size (Figure 3d). The colony morphology and cell morphology defects could be complemented by the expression of *sepI* or a *sepI-gfp* fusion from P_{sepI} in the Δ*sepI* mutant (Figure 3c). Furthermore, SepI-GFP was localized in the septa and as rings at the mid-cell in the Δ*sepI* mutant background (Figure 2b). Additionally, the cell area of the WT expressing *sepI-gfp* from P_{sepI} was decreased in comparison to the Δ*sepI* mutant or the WT (Figure 3d), which adds support to a role of SepI in cell size regulation. Diazotrophic growth of Δ*sepI* was not complemented by the wild type *sepI* gene expressed from P_{sepI}. We note that since we were able to isolate two independent mutant clones with the same phenotype it is unlikely that the inability of diazotrophic growth was due to a secondary mutation. An alternative explanation for the lack of complementation may be a negative effect of *sepI* overexpression on heterocyst differentiation by its placement in a replicative plasmid with an unequal copy number per individual cell in the complemented strain, as has been shown previously for other genes (e.g., Nieves-Morión, Lechno-Yossef et al., 2017).

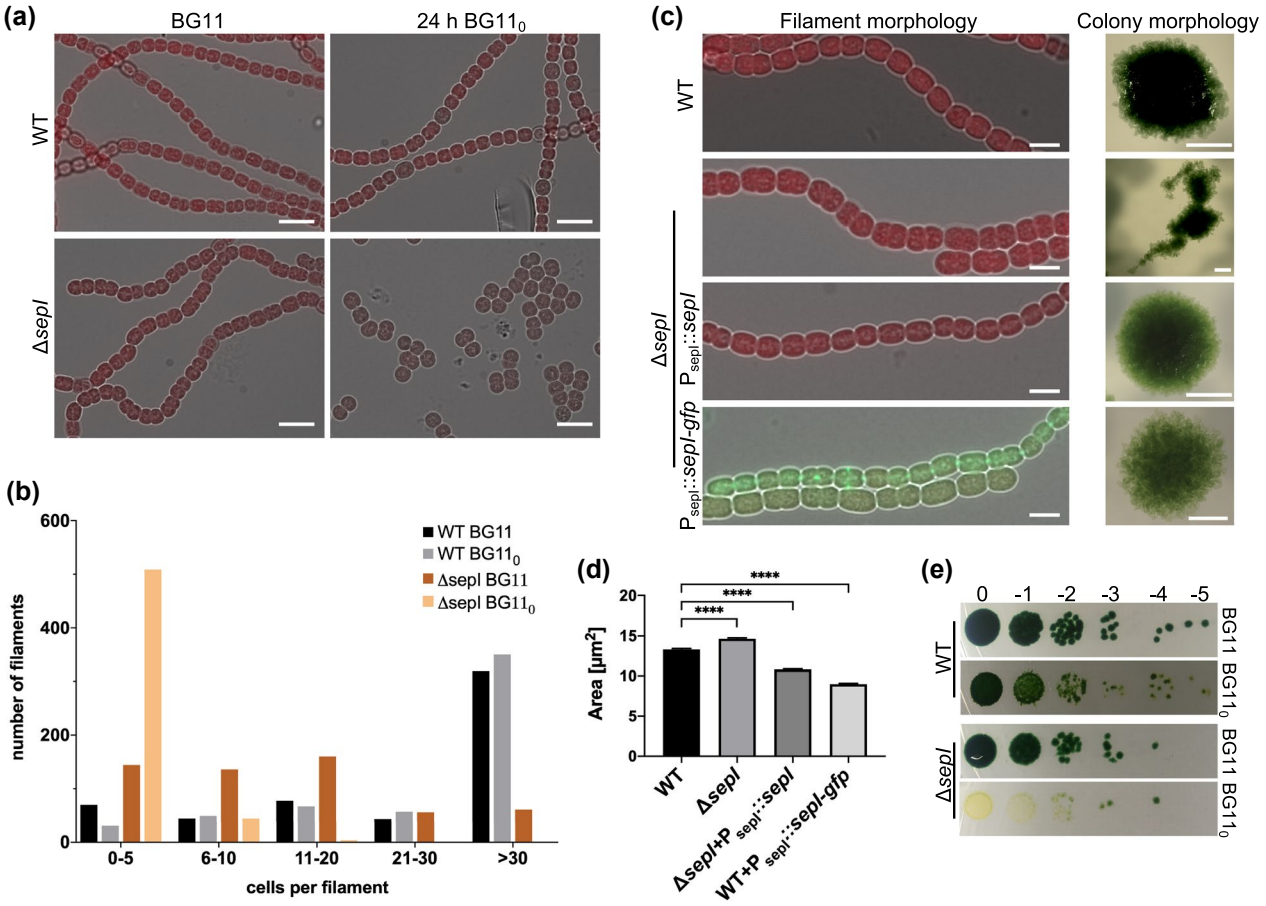

FIGURE 3 SepI is involved in filament integrity and cell and colony morphology. (a) Merged chlorophyll autofluorescence and bright field micrographs of *Anabaena* wild type and Δ*sepI* mutant strain grown in BG11 liquid medium or 24 hr after transfer to $BG11_0$ liquid medium. Scale bars: 10 µm. (b) Filament lengths (in cells per filament) of *Anabaena* WT and Δ*sepI* mutant strain grown in BG11 or 24 hr after transfer to $BG11_0$. (c) Micrographs of *Anabaena* WT and Δ*sepI* mutant filaments as well as of Δ*sepI* mutant complemented with pRL25C-based plasmids carrying P_{sepI}::*sepI* or P_{sepI}::*sepI-gfp* grown in liquid BG11 medium (left). Right, micrographs showing colony morphology in solid medium of the respective strains. Scale bars: (left) 5 µm or (right) 500 µm. (d) Cell surface area in µm^2 of *Anabaena* WT, Δ*sepI* mutant, Δ*sepI* mutant expressing SepI from P_{sepI} and *Anabaena* WT expressing SepI-GFP from P_{sepI}. Error bars indicate standard error of the mean (*SEM*) (WT: n = 758; Δ*sepI*: n = 1285; Δ*sepI* + P_{sepI}::*sepI*: n = 1487; WT + P_{sepI}::*sepI-gfp*: n = 749). Values indicated with asterisks are significantly different from the WT. ****: $p < .0001$ (Dunnett's multiple comparison test and one-way ANOVA). (e) Spot assays of *Anabaena* WT and Δ*sepI* mutant strain. Both strains were grown on BG11 plates, resuspended in BG11 liquid medium and adjusted to an OD_{750} of 0.4 and spotted in triplicates of serial 10-fold dilutions on BG11 or $BG11_0$ plates. Note: re-streaking of green colonies that arose in higher dilutions of the Δ*sepI* mutant grown on $BG11_0$ still exhibited a diazotrophic growth defect and were not spontaneous revertant mutants

2.4 | SepI is involved in septal nanopore formation and intercellular molecular transfer

A defect in filament integrity is commonly observed in mutants of genes encoding proteins that function in the septal junctions (e.g., FraC, FraD and SepJ; Herrero et al., 2016). Additionally, mutant strains of such genes are characterized by a decreased number of nanopores in the septal PG disks and a decreased efficiency of intercellular molecular transfer (Nürnberg et al., 2015). To test if the Δ*sepI* mutant is characterized by similar properties, we isolated the PG layer (i.e., the sacculi) from *Anabaena* wild type and the Δ*sepI* mutant. In addition, we measured the diffusion through septal junctions using the fluorescent markers calcein and 5-carboxyfluorescein (5-CF). In the Δ*sepI* mutant, two different perforation types in the septal PG disks were observed, some with a tiny diameter (in "sealed disks") and others with a very large diameter (defining "unsealed disks") (Figure 4a). Although we cannot exclude that unsealed disks correspond to not yet fully divided cells and would eventually become normal septal disks (see Figure S5 in (Bornikoel, Staiger, Madlung, Forchhammer, & Maldener, 2018)), it should be noted that we rarely observed such large perforations in

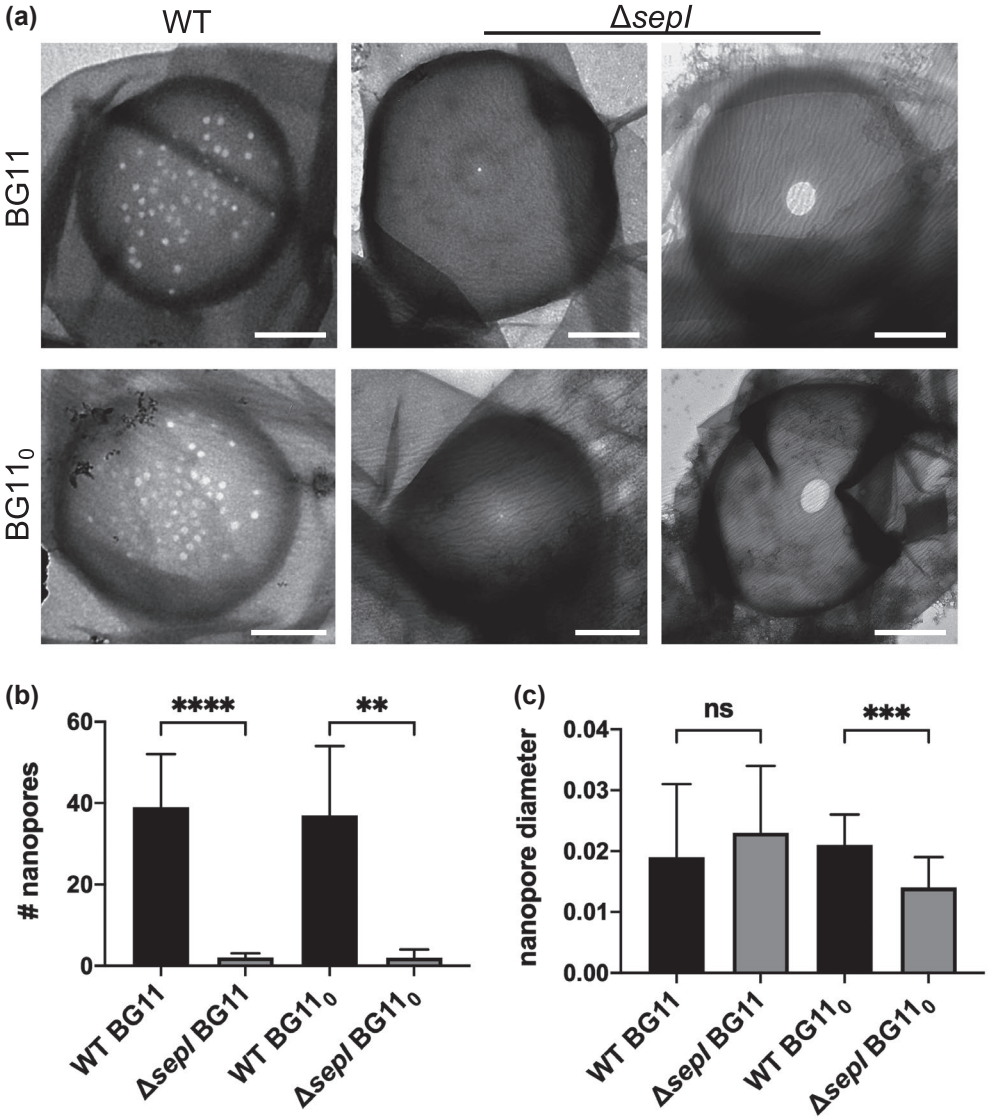

FIGURE 4 Altered nanopore formation in the Δ*sepI* mutant. (a) Representative transmission electron microscopy micrographs of *Anabaena* WT and Δ*sepI* mutant septal PG disks showing nanopore formations. Scale bars 0.5 μm. Note the presence in the mutant of "sealed" (middle panels) and "unsealed" (right panels) septal disks. (b) Number of nanopores per septal PG disk in *Anabaena* WT and Δ*sepI* mutant grown in BG11 or BG11$_0$. Number of recorded septal discs (n): *Anabaena* WT BG11, n = 11; Δ*sepI* BG11, n = 13; *Anabaena* WT BG11$_0$, n = 9; Δ*sepI* BG11$_0$, n = 3. Only "sealed" septal disks were counted. (c) Nanopore diameter in μm for *Anabaena* WT and Δ*sepI* mutant grown in BG11 or BG11$_0$. Number of nanopores analyzed (n): *Anabaena* WT BG11, n = 100; Δ*sepI* BG11, n = 26; *Anabaena* WT BG11$_0$, n = 108; Δ*sepI* BG11$_0$, n = 7. Data correspond only to "sealed" PG disks. For (b) and (c): the significance of the differences in nanopore number and size between mutant and wild type were assessed by the Student's *t* test: $^{**}p < .005$, $^{***}p < .0005$, $^{****}p < .0001$. ns indicates no significant difference. Error bars indicate standard deviation

the wild type. The septal disks with those large perforations were not included in the measurement of nanopore numbers and diameter. The number of nanopores was strongly reduced in the Δ*sepI* mutant and we never observed more than four nanopores in any of the isolated sacculi, regardless of the availability of combined nitrogen. This observation should be compared to about 40 nanopores per septal PG disk in the wild-type grown under the same conditions (Figure 4a,b). Nanopore diameter was unaffected in the Δ*sepI* mutant in BG11 medium but slightly (although significantly) reduced in the Δ*sepI* mutant under nitrogen deprivation (Figure 4c). Using FRAP analysis, we studied the intercellular transfer of calcein and 5-CF between vegetative cells of filaments incubated in the absence of combined nitrogen for 48 hr. The recovery rate constants (*R*) for calcein and 5-CF were decreased in the Δ*sepI* mutant compared to the wild type (Figure 5a). Notably, the decrease in *R* was accompanied by an increased number of noncommunicating cells ($R < 0.01\ s^{-1}$) for the two markers (Figure 5b). We suggest that the two populations of cells in the Δ*sepI* mutant may correspond to cells with sealed or unsealed septal PG disks (see Discussion).

2.5 | SepI localization is explained by interaction with divisome proteins and SepJ

The absence of TM domains in SepI led us to hypothesize that its localization to the Z-ring and septal junctions is due to an interaction with other proteins. To examine that possibility, we tested for an interaction of SepI with several divisome or septal junction-related proteins using an array of bacterial adenylate cyclase two-hybrid (BACTH) assays. Our results showed that SepI specifically interacts with ZipN (a cyanobacterial FtsZ membrane-tethering protein), SepF, SepJ and weakly with FtsI (Figure 6a). No interaction was detected with FtsZ, FtsQ, FtsK, FtsW, FtsK, FtsE, MreB, Ftn6, MinC, FraC, FraD or the filament forming and septal-localized CCRP All4981 (Supplementary Figure S3). Notably, SepI also weakly interacted with the CC domain of SepJ (Figure 6a), suggesting that the CC domains of SepI and SepJ are involved in the interaction of both proteins. We further confirmed the interaction of SepI with ZipN (50% coverage), SepF (37% coverage) and SepJ (6% coverage) using extracts from *Anabaena* cells expressing P_{sepI}::*sepI-gfp* and anti-GFP co-immunoprecipitations followed by LC-MS/MS analytics (Figure 6b). This approach also identified several other CC domain-containing protein interactors of SepI (Figure 6b).

Inspired by its interaction with SepJ, we also investigated the localization pattern of a SepJ-YFP fusion protein in the Δ*sepI* mutant but found no difference in SepJ-YFP localization compared to the wild type (Supplementary Figure S4). Additionally, we also did not find alterations of FtsZ localization in the Δ*sepI* mutant, regardless of the availability of combined nitrogen (Supplementary Figure S5). The Z-ring localization of SepI remains therefore best explained by its interaction with ZipN and SepF, while its localization at the septa could be explained by an interaction with SepJ.

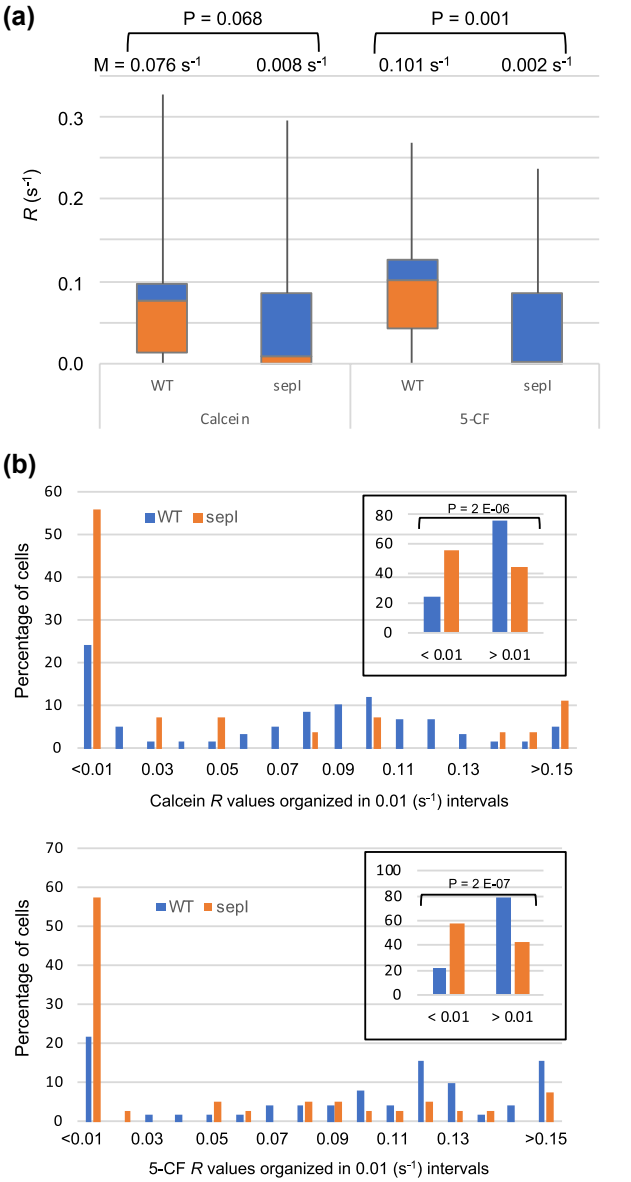

FIGURE 5 Decreased fluorescence recovery rate and non-communicating cells in the Δ*sepI* mutant. (a) Recovery rate constants of fluorescence recovery after photobleaching (FRAP) experiments for calcein- and 5-CF-labelled vegetative cells of *Anabaena* WT and the Δ*sepI* mutant 48 hr after transfer to $BG11_0$ liquid medium. Number of recorded bleached cells (n): calcein PCC 7120 (WT), 57; calcein *alr3364* (*sepI*), 27; 5-CF PCC 7120 (WT), 51; 5-CF *alr3364* (*sepI*), 40. Data are depicted as boxplots (Krzywinski & Altman, 2014a). Orange, quartile group 2 (from Q1 to median); blue, quartile group 3 (from median to Q3). Median values (M) are indicated for each strain and marker. The significance of the difference between mutant and wild type was assessed by the non-parametric Mann-Whitney *U* test (Krzywinski & Altman, 2014b) (P values are indicated on the top). (b) Distribution of cells of *Anabaena* WT (blue) and the Δ*sepI* mutant (orange) showing different *R* values. The percentage of cells within *R* value intervals of $0.01\ s^{-1}$ (i.e., <0.01; from 0.01 to 0.02; from 0.02 to 0.03; etc.; >0.15) was plotted for the transfer of calcein (top) and 5-CF (bottom). The insets show the distribution of cells with $R < 0.01\ s^{-1}$ and $R > 0.01\ s^{-1}$. The significance of the difference of this distribution between the mutant and the wild type was assessed by the χ^2 test (P indicated on top)

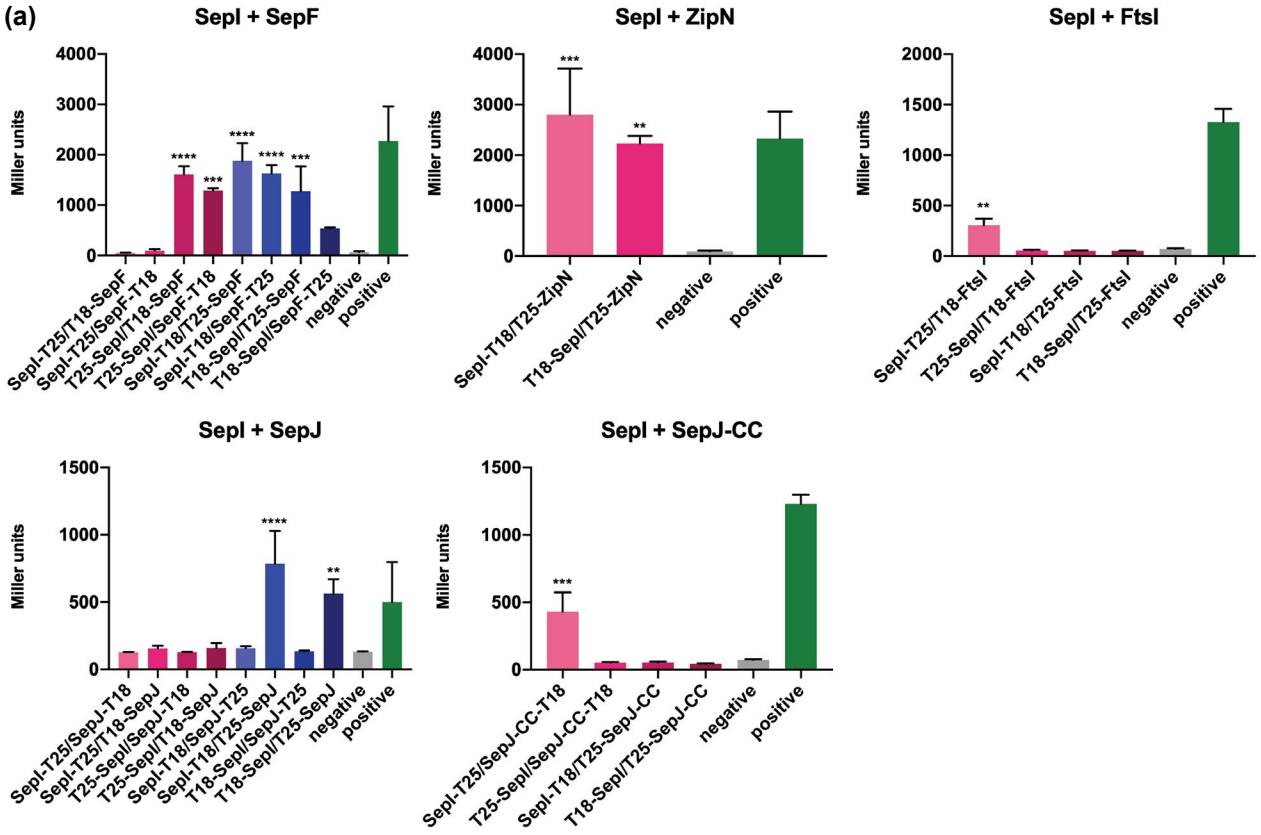

(b)

Accession	Description	Features
All2707	ZipN	TM protein, DnaJ-like
Alr0487	SepF	Cytoplasmic (amphiphatic helix)
Alr2338	SepJ	Coiled coil TM protein
Alr0094	MurI (Glutamate racemase)	In *amiC1-amiC2-murI* operon
Alr3639	possibly phycobilisome peptide	Membrane anchored protein
All7382	MscS (Mechanosensitive ion channel)	Coiled coil TM protein
Alr3445	hypothetical protein	Membrane anchored protein
All4555	unknown protein	Coiled coil protein
All2702	hypothetical protein	Coiled coil protein

FIGURE 6 SepI-interacting proteins. (a) BACTH assays of *E. coli* BTH101 cells co-expressing indicated T25 and T18 translational fusions of all possible pair-wise combinations of SepI, FtsI, ZipN, SepF, SepJ and the CC domain of SepJ (SepJ-CC). *E. coli* cells were subjected to beta-galactosidase assay in triplicates from three independent colonies grown for 2 d at 20°C. Quantitative values are given in Miller units, and the mean results from three independent colonies are presented. Negative: N-terminal T25 fusion construct of the respective protein co-transformed with empty pUT18C. Positive: Zip/Zip control. Error bars indicate standard deviations ($n = 3$). Values indicated with asterisks are significantly different from the negative control. **$p < .01$, ***: $p < .001$, ****: $p < .0001$ (Dunnett's multiple comparison test and one-way ANOVA). (b) Excerpt of possible specific interactors of SepI-GFP identified by co-immunoprecipitation, their description/annotation and a description of specific features of the interactors. The full list of interactors is shown in Supplementary File 2

2.6 | SepI is involved in PG processing

Because of the interaction of SepI with several divisome-associated proteins, its localization to the Z-ring and the apparent alterations in cell and colony morphology in the Δ*sepI* mutant, we next examined whether PG biogenesis is altered in the Δ*sepI* mutant. For this, we stained *Anabaena* wild type and the Δ*sepI* mutant with HADA, a fluorescently labeled D-amino acid, and a fluorescently labeled vancomycin (Van-FL). HADA stains active sites of transpeptidase activity (Hsu et al., 2017) while Van-FL binds to inserted and non-crosslinked PG precursors (Daniel & Errington, 2003). We found that HADA staining was unaffected in the Δ*sepI* mutant even upon nitrogen stepdown-induced cell morphological changes and filament fragmentation (Figure 7a). Like HADA, Van-FL readily stained the septa and the mid-cell regions of the *Anabaena* filament. Notably, however, Van-FL more readily stained the lateral cell walls of the Δ*sepI* mutant than the WT, especially when

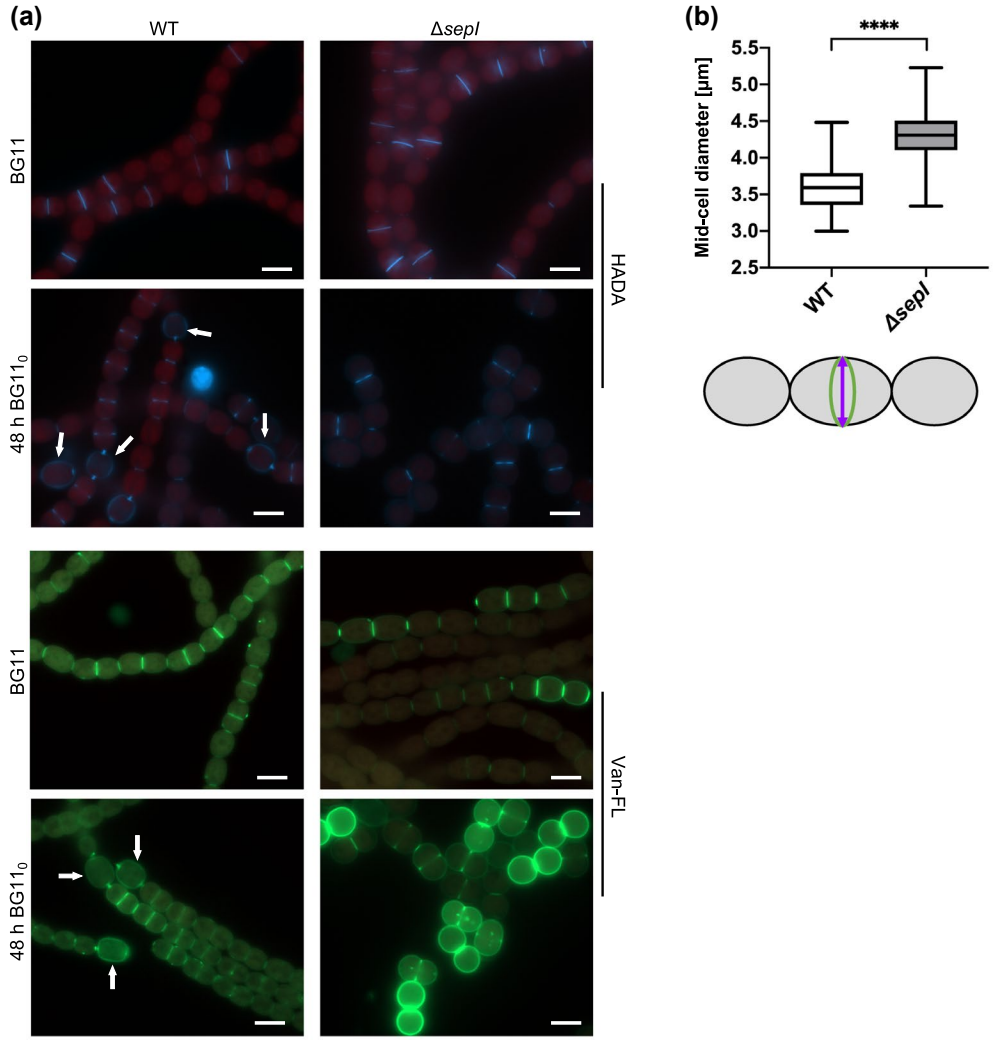

FIGURE 7 SepI is involved in PG biogenesis and septum diameter determination. (a) Merged chlorophyll autofluorescence and HADA or Van-FL fluorescence micrographs of *Anabaena* WT and Δ*sepI* mutant strain grown in BG11 or 48 hr after transfer to BG11$_0$. White arrows indicate heterocysts. Scale bars: 5 µm. (b) Measurement of mid-cell diameter determined from HADA-labeled *Anabaena* WT and Δ*sepI* mutant cells grown in BG11. Lower part shows a depiction of measured rings within an *Anabaena* filament. Green indicates a fully developed PG-ring and the purple arrow indicates the measured distance that is plotted on the upper part. Error bars indicate standard deviations (*Anabaena* WT: n = 600; Δ*sepI* mutant: n = 630)

incubated in BG11$_0$ medium. In the *Anabaena* WT, lateral cell wall staining could be readily observed in heterocysts rather than in vegetative cells similar to what has previously been reported for HADA (Zhang, Lin, Xing, & Zhang, 2018). In contrast, 48 hr after nitrogen-stepdown, Van-FL frequently stained the whole cell wall of a large proportion of Δ*sepI* mutant cells (Figure 7a), indicating alterations in nascent PG synthesis. As we consistently observed an increase in cell diameter in the Δ*sepI* mutant (Figure 3c,d and Figure 7a), we measured mid-cell diameter (determined as HADA-stained rings) in *Anabaena* wild type and the Δ*sepI* mutant and found that mid-cell diameter was significantly increased in the Δ*sepI* mutant (Figure 7b). Thus, consistent with a role of SepI in the *Anabaena* divisome, these observations suggest that SepI influences PG biogenesis.

3 | DISCUSSION

Based on the presence of an outer membrane, cyanobacteria are generally classified as Gram-negative bacteria. However, cyanobacteria also possess an unusually thick PG sheet between the cytoplasmic and outer membranes that bears similarities with that of Gram-positive bacteria (Hahn & Schleiff, 2014; Hoiczyk & Hansel, 2000). In accordance with their ambiguous cell envelope phenotype, the cyanobacterial divisome has previously been shown to include a combination of Gram-positive-like, Gram-negative-like and cyanobacterial-specific proteins (Koksharova & Wolk, 2002; MacCready et al., 2017; Marbouty, Saguez, et al., 2009; Miyagishima et al., 2005). Here, we identified a novel cyanobacterial divisome-associated protein, SepI (Figure 8), which is ubiquitous in filamentous,

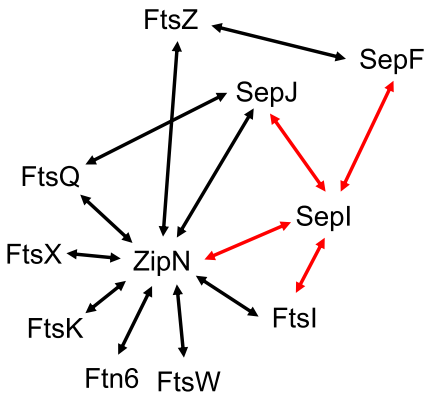

FIGURE 8 Interaction network of known divisome components in *Anabaena*. A model for a partial divisome and septal junction network in *Anabaena* as deduced from BACTH and co-IP analyses. Red arrows indicate interactions identified in the current analysis while interactions indicated with black arrows have been previously described by (Camargo et al., 2019; Ramos-León et al., 2015)

heterocystous cyanobacteria. Moreover, SepI homologs are almost exclusively restricted to this type of cyanobacteria and, as such, it is likely that SepI exudes a specific function in them. SepI localizes to the Z-ring in *Anabaena* but fails to directly interact with FtsZ or to bind FtsZ from *Anabaena* cell-free lysates in pulldown assays. However, we have found evidence for SepI interaction with *Anabaena* Z-ring proteins ZipN and SepF, which could recruit SepI to the divisome.

Deletion of *sepI* resulted in an increase in cell size and enlarged mid-cell diameter, processes governed by the divisome (den Blaauwen et al., 2017). Also, in the Δ*sepI* mutant the pattern of Van-Fl staining was different to that of the wild type. In wild-type *Anabaena*, we found that only heterocyst envelopes are fully labeled with Van-Fl, while vegetative cells mostly show septal or mid-cell Van-Fl staining as previously shown (Lehner et al., 2013). In contrast, in the Δ*sepI* mutant, many cell envelopes were fully labeled with Van-Fl, which could indicate that in these cells PG biogenesis is disturbed. This is consistent with a direct interaction, observed in our BACTH assays, of SepI with FtsI, an essential septal transpeptidase in *Anabaena* (Burnat, Schleiff, & Flores, 2014). Furthermore, the observed increased mid-cell diameter and large perforations in some septal PG disks, which may correspond to unsealed disks, may be related to a slow closing of septal PG in the Δ*sepI* mutant, indicating a role of SepI in septal PG remodeling including nanopore formation and septal junction localization.

A function of SepI in the septal junctions, including septal junction integrity, is supported by filament fragility, abnormal nanopore formation in the Δ*sepI* mutant, and possible physical interaction with SepJ. This notion is reminiscent of the role of the septal proteins SepJ, FraC and FraD that are needed for filament integrity (Flores et al., 2007; Merino-Puerto et al., 2010; Nayar et al., 2007). Similar to the Δ*sepJ* mutant, the Δ*sepI* mutant failed to differentiate heterocysts under nitrogen-deprivation. Thus, we termed Alr3364 "SepI" to highlight its involvement in septal junction biology. SepI-GFP localized to the Z-ring and the septa of vegetative cells, reminiscent of SepJ-GFP (Flores et al., 2007). In accordance to the previously described lack of Z-rings in heterocysts (Kuhn, Peng, Bedu, & Zhang, 2000), we never observed SepI resembling a Z-ring in heterocysts as well. Like in the *sepJ*, *fraC* and *fraD* mutants, we detected a defect in direct cell-cell transfer of calcein and 5-CF as investigated by FRAP analysis. Specifically, we observed an increased number of non-communicating cells in the *sepI* mutant. We speculate that non-communicating cells have at both cell poles sealed disks that, according to the low number of nanopores in the mutant, may contain few functional septal junctions. If this were the case, the unsealed disks of the mutant would host a number of functional septal junctions that mediate a significant intercellular transfer of the fluorescent markers. Further work will be necessary to test this hypothesis. Taken together, our results suggest that during cell division, SepI is recruited to the divisome (i.e., the mid-cell) through its interactions with ZipN and SepF, there interacting with FtsI (Figure 8) and possibly influencing its transpeptidase activity. From there, SepI would localize to the new septum, remaining in the mature daughter cells after cytokinesis. Both during septum formation and in the mature septa connecting daughter cells, SepI would influence septal junction biology, including interactions with SepJ. Thus, similar to SepJ (Camargo et al., 2019; Ramos-León et al., 2015), SepI connects the divisome with the septal junctions, thereby providing further support for a dependence on the divisome for septal junction formation.

Whereas the precise topology of SepI cannot be stated with confidence at this stage, the absence of TM domains or signal peptides in SepI and the interaction with the cytoplasmic protein SepF (Camargo et al., 2019) suggests that SepI is also cytoplasmic (Figure 1a). Nonetheless, a possible interaction of SepI with the cytoplasmic membrane cannot be ruled out. Assuming a cytoplasmic localization of SepI would have complex implications in regard to the localization of the N-terminal section of SepJ, including its CC and linker domains. Previous studies have shown that the CC domain of SepJ directly interacts with the PG sheet (Ramos-León et al., 2017) and that SepJ also interacts with the largely periplasmic FtsQ protein (Ramos-León et al., 2015). Thus, the N-terminal part of SepJ, which contains the CC and linker domains, has been placed into the periplasm (Herrero et al., 2016). In our BACTH analysis, SepI strongly interacted with SepJ, regardless of the orientation of the T18 subunit attached to SepI, but only with N-terminally T25-tagged SepJ. Since SepI is likely cytoplasmic, such combination of SepI and SepJ would only allow for an interaction of both proteins if the N-terminus of SepJ is placed in the cytoplasm of the test *E. coli* strain. The moderate interaction strength of SepI with the CC domain of SepJ also supports the idea that the N-terminal CC domain of SepJ is cytoplasmic in the test *E. coli* strain. Whereas these heterologous studies and the co-IP data support an interaction of SepI and SepJ, the topological aspects of this interaction in *Anabaena* remain to be elucidated. Specifically taking into consideration that SepJ is likely processed posttranslationally in *Anabaena* (Ramos-León et al., 2017), this might affect the localization of its domains in the cell and the nature of its interaction with SepI. Notably, the linker sequence of SepJ (Herrero et al., 2016) and the C-terminal non-CC domain of SepI share a similar

amino acid composition. Because amino acid composition positively correlates with similar protein function (Shckorbatov & Berezhnoy, 2008), it is conceivable that both, the C-terminal non-CC domain of SepI and the linker domain of SepJ are involved in similar cellular processes and/or the proteins directly interact through those domains. In summary, we have identified SepI, a novel cyanobacteria-specific CCRP in *Anabaena* that functions in cell size regulation, nanopore formation (perhaps through effects on PG biogenesis), and filament integrity. SepI interacts with known divisome components and SepJ providing further support for a link between the septal junctions and the divisome in *Anabaena*.

4 | MATERIAL AND METHODS

4.1 | Bacterial strains and growth conditions

Anabaena was obtained from the Pasteur Culture Collection (PCC) of cyanobacteria (France). Cells were grown photoautotropically in BG11 or without combined nitrogen ($BG11_0$) at constant light with a light intensity of 30 μmol/m^2/s. When appropriate, 50 μg/ml kanamycin (Km), 5 μg/ml spectinomycin (Sp), 5 μg/ml streptomycin (Sm) or 30 μg/ml neomycin (Nm) was added. *E. coli* strains DH5αMCR and XL1-blue and HB101 were used for cloning and conjugation. *Anabaena* was transformed by conjugation with *E. coli* according to (Ungerer & Pakrasi, 2016). *E. coli* strain BTH101 was used for BACTH assays and *E. coli* BL21 (DE3) was used for expression of His_6 and GFP-tagged proteins in *E. coli*. All *E. coli* strains were grown in LB medium containing the appropriate antibiotics at standard concentrations.

4.2 | Plasmid and strain constructions

All employed plasmids generated in this study were verified by Sanger sequencing (Eurofins) and all primers used for plasmid construction and RT-PCR are listed in Supplementary Table S3. For pCSEL24-nptII, *nptII*, including its promoter, was amplified from pRL25C using primers #43/#44, cut with BamHI and then ligated into BamHI-digested pCSEL24 by Quick Ligase (NEB). For pTHS134 (pKNT25, P_{lac}::*sepI-T25*), *sepI* was amplified from *Anabaena* gDNA using primers #15/#16 and ligated into linearized pKNT25 (using primers #9/#10) by Gibson assembly. For pTHS135 (pKT25, P_{lac}::*T25-sepI*), *sepI* was amplified from *Anabaena* gDNA using primers #17/#18 and ligated into linearized pKT25 (using primers #11/#12) by Gibson assembly. For pTHS136 (pUT18, P_{lac}::*sepI-T18*), *sepI* was amplified from *Anabaena* gDNA using primers #15/#16 and ligated into linearized pUT18 (using primers #9/#10) by Gibson assembly. For pTHS137 (pUT18C, P_{lac}::*T18-sepI*), *sepI* was amplified from *Anabaena* gDNA using primers #19/#20 and ligated into linearized pUT18C (using primers #13/#14) by Gibson assembly. For pTHS138 (pRL25C, P_{petE}::*sepI-gfp*), *sepI* was amplified from *Anabaena* gDNA using primers #23/#24 and ligated into linearized pTHS1 (using primers #21/#22) by Gibson assembly. For pTHS139 (pRL25C, P_{sepI}::*sepI*), *sepI* was amplified from *Anabaena* gDNA using primers #25/#26 and ligated into BamHI and EcoRI-digested pRL25C by Gibson assembly. For pTHS140 (pRL25C, P_{sepI}::*sepI-gfp*), P_{sepI} was amplified from *Anabaena* gDNA using primers #25/#27 and ligated into BamHI and EcoRI-digested pRL25C by Gibson assembly together with *sepI-gfp*, which was amplified from pTHS138 using primers #28/#29. For pTHS141 (pRL25C, P_{sepI}::*sepI-alr3365-alr3366*), P_{sepI}::*sepI-alr3365-alr3366* was amplified from *Anabaena* gDNA using primers #25/#30 and ligated into BamHI and EcoRI-digested pRL25C by Gibson assembly. For pTHS142 (pCSEL24-nptII, P_{sepI}::*sepI*), P_{sepI}::*sepI* was amplified from *Anabaena* gDNA using primers #31/#26 and ligated into EcoRI-digested pCSEL24-nptII by Gibson assembly.For pTHS144 (pRL278, Δ*sepI*::CS3), 1000 bp upstream and 1000 bp downstream of *sepI* were amplified from *Anabaena* gDNA using primers #32/#33 and #36/#37 respectively, and ligated into SacI and XhoI-digested pRL278 flanking the CS3 cassette, which was amplified by primers #34/#35 from pCSEL24, by Gibson assembly. For pTHS147 (pRL25C, P_{sepJ}::*sepJ-yfp*), P_{sepJ}::*sepJ* was amplified from *Anabaena* gDNA using primers #38/#39 and ligated into BamHI and EcoRI-digested pRL25C together with *myc-eyfp*, initially amplified using primers #40/#42 and then extended using primers #41/#42, by Gibson assembly. For pCSS248 and pCSS249 (pKNT25, P_{lac}::*T25-sepJ-CC*; pUT18, P_{lac}::*sepJ-CC-T18*), *sepJ-CC* was amplified using primers #45/#46 and ligated into BamHI and KpnI-digested pKNT25 or pUT18. For the generation of the Δ*sepI* mutant strains, plasmid pTHS144 was conjugated into *Anabaena* WT using triparental mating and exconjugants were re-streaked on BG11 Sm/Sp plates for two rounds of re-streaking. Absence of *sepI* was verified by colony PCR using primers #3 and #4 as well as by RT-PCR of isolated and reverse transcribed RNA from the Δ*sepI* mutant.

4.3 | Computational prediction

Protein domains were investigated using NCBI Conserved Domains Search (Marchler-Bauer et al., 2016) and COILS (V. 2.2) (Lupas, Van Dyke, & Stock, 1991). Subcellular localizations were predicted with TMHMM (V. 2.0) (Sonnhammer, von Heijne, & Krogh, 1998), PSORTb (V. 3.0.2) (Yu et al., 2010), Gneg-mPLoc (V. 2.0) (Shen & Chou, 2010), PSIPRED (V. 4.0) (Buchan & Jones, 2019) and Phobius (Käll, Krogh, & Sonnhammer, 2007). The employed putative promoter site for *sepI* was based on the predictions by BPROM (Solovyev & Salamov, 2011) and was chosen to start 602 bp upstream of *sepI*.

4.4 | Bioinformatic analysis

Homologs to the Anabaena proteins were detected by amino acid sequence similarity using stand-alone BLAST (V. 2.2.26; Altschul, Gish, Miller, Myers, & Lipman, 1990). Protein sequences that were found as BLAST hits with a threshold of *E*-value ≤ 1×10^{-5} were further compared to the *Anabaena* protein by global alignment

using needle (Rice, Longden, & Bleasby, 2000). Hits having ≥ 30% identical amino acids in the global alignment were considered as homologs.

4.5 | Co-immunoprecipitation

For co-immunoprecipitations, *Anabaena* WT or *Anabaena* expressing SepI-GFP from P_{sepI} were grown in BG11 liquid medium. 50 ml cell suspensions were harvested by centrifugation (4800 × *g*, RT, 10 min) and washed 1× in 40 ml Phosphate-buffered saline (PBS; 137 mM NaCl, 2.7 mM KCl, 10 mM phosphate buffer). Anti-GFP co-immunoprecipitation was performed using the μMACS GFP isolation kit (Miltenyi Biotec). For this, *Anabaena* wild type or *Anabaena* expressing SepI-GFP were grown in BG11 medium, pelleted by centrifugation and re-suspended in 1 ml PBS-*N* (PBS supplemented with 1% NP-40) lysis buffers supplemented with a protease inhibitor cocktail (cOmplete™, EDTA-free Protease Inhibitor Cocktail, Sigma-Aldrich). Cells were lysed by bead-beating using a Precellys 24 homogenizer (3 × 30 s, 6500 rpm) (Bertin) and the VK05 lysis kit (Bertin). Cell-free supernatants were then incubated with μMACS anti-GFP microbeads (Miltenyi Biotec) for 30 min on ice and applied to μColumns (Miltenyi Biotec). μColumns were washed 3× with 1 ml PBS-N and proteins were eluted in elution buffer (50 mM Tris HCl (pH 6.8), 50 mM DTT, 1% SDS, 1 mM EDTA, 0.005% bromphenol blue, 10% glycerol).

4.6 | Mass spectrometry

Co-precipitated proteins were identified by LC-MS/MS analytics. For this, coomassie stained gel bands were excised and proteins were reduced with 10 mM DTT at 56°C for 45 min and then alkylated with 55 mM iodoacetamide at room temperature (RT) for 30 min in the dark. The bands were washed with 50 mM ammonium bicarbonate and then dehydrated using acetonitrile. Proteins were digested with 5 ng/μl trypsin in 25 mM ammonium bicarbonate and the gel bands were rehydrated for 5 min at 37°C and proteins were digested over night at 37°C. The next day, samples were acidified with 10% formic acid and the supernatant was transferred into a new reaction tube. Subsequently, 5% formic acid was added to the gel bands and incubated for 10 min, which were then sonicated for 1 min in ice-cooled water and the supernatant was combined with the one from the step before. This was followed by two additional extraction steps with 60% acetonitrile/1% formic acid and 100% acetonitrile, which were performed in the same manner. The combined supernatants were dried in the SpeedVac and the samples were reconstituted in 30 μl 3% acetonitrile/0.1% trifluoroacetic acid. LC-MS/MS analysis was performed using a Dionex U3000 nanoUHPLC (Thermo Fischer Scientific) coupled to a Q Exactive Plus mass spectrometer (Thermo Fischer Scientific). The following LC-MS/MS parameters were applied: 6 μl were injected and loaded on a trap column (Acclaim Pepmap 100 C18, 10 mm × 300 μm, 3 μm, 100 Å, Dionex) and washed for 3 min with 2% ACN/0.05% TFA at a flow-rate of 30 μl/min. Separation was performed using an Acclaim PepMap 100 C18 analytical column (50 cm × 75 μm, 2 μm, 100 Å, Dionex) with a flow-rate of 300 nl/min and following eluents: A (0.05% FA) and B (80% ACN/0.04% FA); linear gradient 5%–40% B in 60 min, 50%–90% B in 5 min, 90% B for 10 min, 90%–5% B in 1 min and equilibrating at 5% B for 11 min. Ionization was performed with 1.5 kV spray voltage applied on a non-coated PicoTip emitter (10 μm tip size, New Objective, Woburn, MA) with the source temperature set to 250°C. The MS data were acquired from 5 to 85 min with MS full scans between 300 and 1,800 m/z at a resolution of 70,000 at m/z 200. The 10 most intense precursors with charge states ≥ 2+ were subjected to fragmentation with HCD with NCE of 27%; isolation width of 3 m/z; resolution, 17,500 at m/z 200. Dynamic exclusion for 30 s was applied with a precursor mass tolerance of 10 ppm. Lock mass correction was performed based on the polysiloxane contaminant signal of 445.120025 m/z. In between runs, wash runs were performed to reduce carry over while cytochrome C was used to monitor mass accuracy and LC quality control. The acquired MS/MS data were searched with the SequestHT algorithm against the entire reviewed Uniprot protein database of *Nostoc* sp. PCC 7,120 (i.e., *Anabaena*) including its large plasmids (6,922 sequences in total). Static modifications applied were carbamidomethylation on cysteine residues, while oxidation on methionine residues was set as dynamic modification. Spectra were searched with full enzyme specificity. A MS mass tolerance of 10 ppm and a MS/MS tolerance of 0.02 Da was used. Proteins with at least three unique peptides were identified with a FDR confidence ≤ 0.01 (high).

4.7 | RNA isolation and RT-PCR

Total RNA was isolated in triplicates from 10 ml *Anabaena* WT or Δ*sepI* mutant cultures using the Direct-zol™ RNA MiniPrep Kit (Zymo Research) according to the manufacturer's instructions. Cells were lysed with VK05 lysis tubes (Bertin). Isolated RNA was treated with DNA-free™ Kit (2 units rDNAs/reaction; Thermo Fischer Scientific) and 200 ng RNA was reverse transcribed using the qScript™ cDNA Synthesis Kit (Quanta Biosciences). RT-PCRs of cDNA samples for *rnpB*, *sepI*, *alr3365*, *alr3366*, *sepI* + *alr3366* and *sepI* + *alr3365* were done using primer pairs #1/#2, #3/#4, #5/#6, #7/#8, #3/#8 or #3/#6 respectively (Primers are listed in Supplementary Table S3).

4.8 | Microscopy

Bacteria were immobilized on a 2% low-melting agarose in PBS agarose pad and air dried before microscopic analysis. Epifluorescence microscopy was performed using an Axio Imager.M2 light microscope (Carl Zeiss) equipped with Plan-Apochromat 63x/1.40 Oil M27 objective and the AxioCam MR R3 imaging device (Carl Zeiss). GFP, Alexa Fluor 488 and YFP fluorescence was imaged using filter set 38 (Carl Zeiss; excitation: 470/40 nm band pass (BP) filter; emission:

525/50 nm BP). Chlorophyll autofluorescence was detected with filter set 15 (Carl Zeiss; excitation: 546/12 nm BP; emission: 590 nm long pass). Colony morphologies were documented with a Leica KL 200 LED microscope. For DAPI staining of intracellular DNA, cells were incubated in the dark at RT for about 5 min with 20 μg/ml DAPI in PBS. DAPI fluorescence was visualized with filter set 49 (Carl Zeiss; excitation: G 365 nm; emission: 455/50 nm). Filament length (cells per filament), cell area, roundness and septum diameter were recorded using the ImageJ 1.52a imaging software of microscopy images generated using the Zen Blue software (Zeiss). Statistical tests and plotting of data were performed with the GraphPad Prim 8.1.2 software.

4.9 | FRAP analysis

For FRAP analysis, calcein and 5-carboxyfluorescein staining was performed as previously reported (Merino-Puerto et al., 2011; Mullineaux et al., 2008). Cell suspensions were then spotted onto agar and placed in a temperature-controlled sample holder with a glass cover slip on top. All measurements were carried out at 30°C. Cells were imaged with a Leica HCX PL Apo 63×, 1.4-NA oil immersion objective attached to a Leica TCS SP2 confocal laser-scanning microscope with a 488-nm line argon laser as the excitation source. Fluorescent emission was monitored by collection across windows of 500 to 520 nm and a 150-μm pinhole. After an initial image was recorded, the bleach was carried out by an automated FRAP routine as previously reported (Mullineaux et al., 2008). For FRAP data analysis, kinetics of transfer of the fluorescent tracer was quantified and the recovery constant, *R*, was calculated as previously described (Nieves-Morión, Lechno-Yossef et al., 2017).

4.10 | Nanopore analysis

Filaments grown in BG11 medium (with Sm/ Sp for the mutant) to about 5 to 8 μg Chl/ml were washed and incubated in BG11 and $BG11_0$ medium for 24 hr. The filaments were harvested by centrifugation and the sacculi were isolated and analyzed as described previously (Lehner et al., 2013; Nürnberg et al., 2015). The purified sacculi were deposited on formvar/carbon film coated copper grids, and stained with 1% (w/v) uranyl acetate. All the samples were examined with a Zeiss Libra 120 Plus electron microscope at 120 kV.

4.11 | Immunofluorescence

Localization of FtsZ in *Anabaena* WT and Δ*sepI* mutant strain was detected by immunofluorescence according to Ramos-León et al. (2015) using rabbit anti-FtsZ primary antibody (Agrisera; raised against *Anabaena* FtsZ; 1:250 diluted) followed by incubation with 7.5 μg/ml Alexa Fluor 488-conjugated goat anti-rabbit IgG (H + L) secondary antibody (Thermo Fischer Scientific).

4.12 | HADA and Van-FL labeling

For Van-FL labeling of *Anabaena* WT and the Δ*sepI* mutant, cells were grown in BG11 or transferred to $BG11_0$ for 2 days, washed three times in BG11 or $BG11_0$ and incubated with 5 μg/ml Van-FL (final concentration). Cells were then incubated in the dark for 1 h at 30°C. For HADA labeling, *Anabaena* WT and Δ*sepI* mutant were grown in BG11 liquid medium, washed three times in BG11 or $BG11_0$ and incubated with 0.2 μM HADA in BG11 or $BG11_0$ for 2 days at standard growth conditions. Prior visualization of HADA and Van-FL-stained cells, cells were washed three times with PBS. We note: washing the cells prior addition of HADA greatly increases the labeling efficiency.

4.13 | Bacterial two-hybrid assays

For the analysis of protein-protein interactions, the BACTH system (Euromedex) was employed. Gene candidates were cloned into the expression vectors pKNT25, pKT25, pUT18 and pUT18C by GIBSON assembly or by conventional restriction enzyme-based cloning techniques, thereby generating C- and N-terminal translational fusions to the T25 or T18 subunit. *E. coli* BTH101 cells were co-transformed with 5 ng of the indicated plasmids, plated onto LB plates supplemented with 200 μg/ml X-gal, 0.5 mM IPTG, Amp, Km and grown at 30°C for 24–36 hr. Interactions were quantified by beta-galactosidase assays from three independent colonies for each combination according to Karimova, Davi, and Ladant (2012). For this aim, cultures were grown for 2 d at 20°C in LB Amp, Km, 0.5 mM IPTG and interaction strength of the investigated proteins was quantified by beta-galactosidase-mediated hydrolyzation of ONPG (ortho-Nitrophenyl-β-galactosidase) recorded in Miller units as described in the manufacturer's manual (Euromedex).

4.14 | Spot assay

Defects in cell viability were evaluated by spot assays as described by Springstein et al. (2020). *Anabaena* WT and Δ*sepI* mutant strain were grown on BG11 plates, resuspended in BG11 medium and adjusted to an OD_{750} of 0.4. 5 μl of 10-fold dilutions of cells were spotted in triplicates onto BG11 or $BG11_0$ plates and incubated under standard growth conditions until no further colonies arose in the highest dilution.

ACKNOWLEDGEMENTS

We thank Katrin Schumann and Marius Lasse Theune for their assistance in the experimental work, and Silvia Picossi for construction of the T18- and T25-fussions to the SepJ-coiled-coil and linker sequences. The study was supported by the German science foundation (DFG) (grant no. STU513/2-1 awarded to KS). Work in Seville was supported by grants no. BFU2016-77097-P (to AH) and BFU2017-88202-P (to EF) from the Spanish Government co-financed by the European Regional Development Fund.

COMPETING INTERESTS

The authors declare no competing interests.

AUTHOR CONTRIBUTIONS

All authors designed and discussed the study. BLS, SA and AOD performed the experiments. TD performed the comparative genomics analysis. BLS drafted the manuscript with contributions from all coauthors. BLS, KS, AH, EF and TD directed the research together.

DATA AVAILABILITY STATEMENT

All data generated or analyzed during this study are included in this published article (and its supplementary information files). The datasets generated during and/or analyzed during the current study are available from the corresponding authors on reasonable request.

ORCID

Benjamin L. Springstein https://orcid.org/0000-0002-3461-5391
Antonia Herrero https://orcid.org/0000-0003-1071-6590
Karina Stucken https://orcid.org/0000-0002-2783-4342
Enrique Flores https://orcid.org/0000-0001-7605-7343
Tal Dagan https://orcid.org/0000-0002-9042-192X

REFERENCES

Altschul, S. F., Gish, W., Miller, W., Myers, E. W., & Lipman, D. J. (1990). Basic local alignment search tool. *Journal of Molecular Biology*, *215*, 403–410. https://doi.org/10.1016/S0022-2836(05)80360-2

Bornikoel, J., Carrión, A., Fan, Q., Flores, E., Forchhammer, K., Mariscal, V., … Maldener, I. (2017). Role of two cell wall amidases in septal junction and nanopore formation in the multicellular Cyanobacterium *Anabaena* sp. PCC 7120. *Frontiers in Cellular and Infection Microbiology*, *7*, 386. https://doi.org/10.3389/fcimb.2017.00386

Bornikoel, J., Staiger, J., Madlung, J., Forchhammer, K., & Maldener, I. (2018). LytM factor Alr3353 affects filament morphology and cell–cell communication in the multicellular cyanobacterium *Anabaena* sp. PCC 7120. *Molecular Microbiology*, *108*, 187–203.

Buchan, D. W. A., & Jones, D. T. (2019). The PSIPRED protein analysis workbench: 20 years on. *Nucleic Acids Research*, *47*, W402–W407. https://doi.org/10.1093/nar/gkz297

Burnat, M., Schleiff, E., & Flores, E. (2014). Cell envelope components influencing filament length in the heterocyst-forming cyanobacterium *Anabaena* sp. strain PCC 7120. *Journal of Bacteriology*, *196*, 4026–4035. https://doi.org/10.1128/JB.02128-14

Camargo, S., Picossi, S., Corrales-Guerrero, L., Valladares, A., Arévalo, S., & Herrero, A. (2019). ZipN is an essential FtsZ membrane tether and contributes to the septal localization of SepJ in the filamentous cyanobacterium *Anabaena*. *Scientific Reports*, *9*, 1–15. https://doi.org/10.1038/s41598-019-39336-6

Claessen, D., Rozen, D. E., Kuipers, O. P., Søgaard-Andersen, L., & Wezel, G. P. V. (2014). Bacterial solutions to multicellularity: A tale of biofilms, filaments and fruiting bodies. *Nature Reviews Microbiology*, *12*, 115–124. https://doi.org/10.1038/nrmicro3178

Corrales-Guerrero, L., Camargo, S., Valladares, A., Picossi, S., Luque, I., Ochoa De Alda, J. A. G., & Herrero, A. (2018). FtsZ of filamentous, heterocyst-forming cyanobacteria has a conserved N-terminal peptide required for normal FtsZ polymerization and cell division. *Frontiers in Microbiology*, *9*, 1–20. https://doi.org/10.3389/fmicb.2018.02260

Daniel, R. A., & Errington, J. (2003). Control of cell morphogenesis in bacteria: Two distinct ways to make a rod-shaped cell. *Cell*, *113*, 767–776. https://doi.org/10.1016/S0092-8674(03)00421-5

den Blaauwen, T., Hamoen, L. W., & Levin, P. A. (2017). The divisome at 25: The road ahead. *Current Opinion in Microbiology*, *36*, 85–94. https://doi.org/10.1016/j.mib.2017.01.007

Elhai, J., & Wolk, C. (1988). A versatile class of positive-selection vectors based on the nonviability of palindrome-containing plasmids that allows cloning into long polylinkers. *Gene*, *68*, 119–138. https://doi.org/10.1016/0378-1119(88)90605-1

Flores, E., Herrero, A., Forchhammer, K., & Maldener, I. (2016). Septal junctions in filamentous heterocyst-forming cyanobacteria. *Trends in Microbiology*, *24*, 79–82. https://doi.org/10.1016/j.tim.2015.11.011

Flores, E., Nieves-Morión, M., & Mullineaux, C. (2018). Cyanobacterial septal junctions: Properties and regulation. *Life*, *9*, 1. https://doi.org/10.3390/life9010001

Flores, E., Pernil, R., Muro-Pastor, A. M., Mariscal, V., Maldener, I., Lechno-Yossef, S., … Herrero, A. (2007). Septum-localized protein required for filament integrity and diazotrophy in the heterocyst-forming cyanobacterium *Anabaena* sp. strain PCC 7120. *Journal of Bacteriology*, *189*, 3884–3890. https://doi.org/10.1128/JB.00085-07

Garcia-Pichel, F., Zehr, J. P., Bhattacharya, D., & Pakrasi, H. B. (2020). What's in a name? The case of cyanobacteria. *Journal of Phycology*, *56*, 1–5. https://doi.org/10.1111/jpy.12934

Hahn, A., & Schleiff, E. (2014). *The cell envelope. In The Biology of Cyanobacteria*. Norfolk, UK: Caister Academic Press.

Herrero, A., Stavans, J., & Flores, E. (2016). The multicellular nature of filamentous heterocyst-forming cyanobacteria. *FEMS Microbiology Reviews*, *40*, 831–854. https://doi.org/10.1093/femsre/fuw029

Hoiczyk, E., & Hansel, A. (2000). Cyanobacterial cell walls: News from an unusual prokaryotic envelope. *Journal of Bacteriology*, *182*, 1191–1199. https://doi.org/10.1128/JB.182.5.1191-1199.2000

Hsu, Y.-P., Rittichier, J., Kuru, E., Yablonowski, J., Pasciak, E., Tekkam, S. … VanNieuwenhze, M. S. (2017). Full color palette of fluorescent d-amino acids for in situ labeling of bacterial cell walls. *Chem Sci*, *8*, 6313–6321.

Käll, L., Krogh, A., & Sonnhammer, E. L. L. (2007). Advantages of combined transmembrane topology and signal peptide prediction-the Phobius web server. *Nucleic Acids Research*, *35*, 429–432. https://doi.org/10.1093/nar/gkm256

Karimova, G., Davi, M., & Ladant, D. (2012). The β-lactam resistance protein Blr, a small membrane polypeptide, is a component of the *Escherichia coli* cell division machinery. *Journal of Bacteriology*, *194*, 5576–5588.

Koksharova, O. A., & Wolk, C. P. (2002). A novel gene that bears a DnaJ motif influences cyanobacterial cell division. *Journal of Bacteriology*, *184*, 5524–5528. https://doi.org/10.1128/JB.184.19.5524-5528.2002

Krzywinski, M., & Altman, N. (2014a). Visualizing samples with box plots. *Nature Methods*, *11*, 119–120. https://doi.org/10.1038/nmeth.2813

Krzywinski, M., & Altman, N. (2014b). Nonparametric tests. *Nature Methods*, *11*, 467–468. https://doi.org/10.1038/nmeth.2937

Kuhn, I., Peng, L., Bedu, S., & Zhang, C.-C. (2000). Developmental regulation of the cell division protein FtsZ in *Anabaena* sp. strain PCC 7120, a cyanobacterium capable of terminal differentiation. *Journal of Bacteriology*, *182*, 4640–4643. https://doi.org/10.1128/JB.182.16.4640-4643.2000

Kumar, K., Mella-Herrera, R. A., & Golden, J. W. (2010). Cyanobacterial heterocysts. *Cold Spring Harb Perspect Biol*, *2*, 1–19. https://doi.org/10.1101/cshperspect.a000315

Lehner, J., Berendt, S., Dörsam, B., Pérez, R., Forchhammer, K., & Maldener, I. (2013). Prokaryotic multicellularity: A nanopore array for bacterial cell communication. *The FASEB Journal*, *27*, 2293–2300. https://doi.org/10.1096/fj.12-225854

Lupas, A., Van Dyke, M., & Stock, J. (1991). Predicting coiled coils from protein sequences. *Science (80-)*, *252*, 1162–1164.

MacCready, J. S., Schossau, J., Osteryoung, K. W., & Ducat, D. C. (2017). Robust Min-system oscillation in the presence of internal photosynthetic membranes in cyanobacteria. *Molecular Microbiology*, *103*, 483–503.

Marbouty, M., Mazouni, K., Saguez, C., Cassier-Chauvat, C., & Chauvat, F. (2009). Characterization of the Synechocystis strain PCC 6803 penicillin-binding proteins and cytokinetic proteins FtsQ and FtsW and their network of interactions with ZipN. *Journal of Bacteriology*, *191*, 5123–5133. https://doi.org/10.1128/JB.00620-09

Marbouty, M., Saguez, C., Cassier-Chauvat, C., & Chauvat, F. (2009). Characterization of the FtsZ-interacting septal proteins SepF and Ftn6 in the spherical-celled cyanobacterium Synechocystis strain PCC 6803. *Journal of Bacteriology*, *191*, 6178–6185. https://doi.org/10.1128/JB.00723-09

Marchler-Bauer, A., Bo, Y., Han, L., He, J., Lanczycki, C. J., Lu, S. … Bryant, S. H. (2016). CDD/SPARCLE: Functional classification of proteins via subfamily domain architectures. *Nucleic Acids Research*, *45*, D200–D203.

Merino-Puerto, V., Mariscal, V., Mullineaux, C. W., Herrero, A., & Flores, E. (2010). Fra proteins influencing filament integrity, diazotrophy and localization of septal protein SepJ in the heterocyst-forming cyanobacterium *Anabaena* sp. *Molecular Microbiology*, *75*, 1159–1170.

Merino-Puerto, V., Schwarz, H., Maldener, I., Mariscal, V., Mullineaux, C. W., Herrero, A., & Flores, E. (2011). FraC/FraD-dependent intercellular molecular exchange in the filaments of a heterocyst-forming cyanobacterium, *Anabaena* sp. *Molecular Microbiology*, *82*, 87–98. https://doi.org/10.1111/j.1365-2958.2011.07797.x

Mitschke, J., Vioque, A., Haas, F., Hess, W. R., & Muro-Pastor, A. M. (2011). Dynamics of transcriptional start site selection during nitrogen stress-induced cell differentiation in *Anabaena* sp. PCC7120. *Proceedings of the National Academy of Sciences*, *108*, 20130–20135. https://doi.org/10.1073/pnas.1112724108

Miyagishima, S. Y., Wolk, P. P., & Osteryoung, K. W. (2005). Identification of cyanobacterial cell division genes by comparative and mutational analyses. *Molecular Microbiology*, *56*, 126–143. https://doi.org/10.1111/j.1365-2958.2005.04548.x

Mullineaux, C. W., Mariscal, V., Nenninger, A., Khanum, H., Herrero, A., Flores, E., & Adams, D. G. (2008). Mechanism of intercellular molecular exchange in heterocyst-forming cyanobacteria. *EMBO Journal*, *27*, 1299–1308. https://doi.org/10.1038/emboj.2008.66

Nayar, A. S., Yamaura, H., Rajagopalan, R., Risser, D. D., & Callahan, S. M. (2007). FraG is necessary for filament integrity and heterocyst maturation in the cyanobacterium *Anabaena* sp. strain PCC 7120. *Microbiology*, *153*, 601–607. https://doi.org/10.1099/mic.0.2006/002535-0

Nieves-Morión, M., Lechno-Yossef, S., López-Igual, R., Frías, J. E., Mariscal, V., Nürnberg, D. J., … Flores, E. (2017). Specific glucoside transporters influence septal structure and function in the filamentous, heterocyst-forming Cyanobacterium *Anabaena* sp. strain PCC 7120. *Journal of Bacteriology*, *199*, e00876–e916. https://doi.org/10.1128/JB.00876-16

Nieves-Morión, M., Mullineaux, C. W., & Flores, E. (2017). Molecular diffusion through cyanobacterial septal junctions. *Mbio*, *8*, 1–5. https://doi.org/10.1128/mBio.01756-16

Nürnberg, D. J., Mariscal, V., Bornikoel, J., Nieves-Morión, M., Krauß, N., Herrero, A., … Mullineaux, C. W. (2015). Intercellular diffusion of a fluorescent sucrose analog via the septal junctions in a filamentous cyanobacterium. *Mbio*, *6*, 1–12. https://doi.org/10.1128/mBio.02109-14

Ramos-León, F., Mariscal, V., Battchikova, N., Aro, E. M., & Flores, E. (2017). Septal protein SepJ from the heterocyst-forming cyanobacterium *Anabaena* forms multimers and interacts with peptidoglycan. *FEBS Open Bio*, *7*, 1515–1526.

Ramos-León, F., Mariscal, V., Frías, J. E., Flores, E., & Herrero, A. (2015). Divisome-dependent subcellular localization of cell-cell joining protein SepJ in the filamentous cyanobacterium *Anabaena*. *Molecular Microbiology*, *96*, 566–580.

Rice, P., Longden, I., & Bleasby, A. (2000). EMBOSS: The European molecular biology open software suite. *Trends in Genetics*, *16*, 276–277. https://doi.org/10.1016/S0168-9525(00)02024-2

Rippka, R., Stanier, R. Y., Deruelles, J., Herdman, M., & Waterbury, J. B. (1979). Generic assignments, strain histories and properties of pure cultures of cyanobacteria. *Microbiology*, *111*, 1–61. https://doi.org/10.1099/00221287-111-1-1

Rudolf, M., Tetik, N., Ramos-León, F., Flinner, N., Ngo, G., Stevanovic, M., … Schleiff, E. (2015). The Peptidoglycan-binding protein SjcF1 influences septal junction function and channel formation in the filamentous Cyanobacterium *Anabaena*. *Mbio*, *6*, e00376–e00415. https://doi.org/10.1128/mBio.00376-15

Shckorbatov, Y., & Berezhnoy, A. (2008). Similarities in protein amino acid composition in connection with principles of protein evolution. *Central European Journal of Biology*, *3*, 205–209. https://doi.org/10.2478/s11535-008-0015-8

Shen, H. B., & Chou, K. C. (2010). Gneg-mPLoc: A top-down strategy to enhance the quality of predicting subcellular localization of Gram-negative bacterial proteins. *Journal of Theoretical Biology*, *264*, 326–333. https://doi.org/10.1016/j.jtbi.2010.01.018

Solovyev, V., & Salamov, A. (2011). Automatic annotation of microbial genomes and metagenomic sequences. In R. W. Li (Ed.), *Metagenomics and its applications in agriculture, biomedicine and environmental studies* (pp. 61–78). Hauppauge, NY: Nova Science Publishers Inc.

Sonnhammer, E. L., von Heijne, G., & Krogh, A. (1998). A hidden Markov model for predicting transmembrane helices in protein sequences. *Proceedings*, *6*, 175–182.

Springstein, B. L., Woehle, C., Weissenbach, J., Helbig, A. O., Dagan, T., & Stucken, K. (2020). Identification and characterization of novel filament-forming proteins in cyanobacteria. *Scientific Reports*, *10*, 1894. https://doi.org/10.1038/s41598-020-58726-9

Ungerer, J., & Pakrasi, H. B. (2016). Cpf1 is a versatile tool for CRISPR genome editing across diverse species of cyanobacteria. *Scientific Reports*, *6*, 1–9. https://doi.org/10.1038/srep39681

Weiss, G. L., Kieninger, A.-K., Maldener, I., Forchhammer, K., & Pilhofer, M. (2019). Structure and function of a bacterial gap junction analog. *Cell*, *178*, 374–384. https://doi.org/10.1016/j.cell.2019.05.055

Wilk, L., Strauss, M., Rudolf, M., Nicolaisen, K., Flores, E., Kühlbrandt, W., & Schleiff, E. (2011). Outer membrane continuity and septosome formation between vegetative cells in the filaments of *Anabaena* sp. PCC 7120. *Cellular Microbiology*, *13*, 1744–1754. https://doi.org/10.1111/j.1462-5822.2011.01655.x

Yu, N. Y., Wagner, J. R., Laird, M. R., Melli, G., Rey, S., Lo, R., … Brinkman, F. S. L. (2010). PSORTb 3.0: Improved protein subcellular localization prediction with refined localization subcategories and predictive capabilities for all prokaryotes. *Bioinformatics*, *26*, 1608–1615. https://doi.org/10.1093/bioinformatics/btq249

Zhang, C.-C.- C., Hugenin, S., Friry, A., Huguenin, S., & Friry, A. (1995). Analysis of genes encoding the cell division protein FtsZ and a glutathione synthetase homologue in the cyanobacterium *Anabaena* sp. PCC 7120. *Research in Microbiology*, *146*, 445–455. https://doi.org/10.1016/0923-2508(96)80290-7

Zhang, J. Y., Lin, G. M., Xing, W. Y., & Zhang, C. C. (2018). Diversity of growth patterns probed in live cyanobacterial cells using a fluorescent analog of a peptidoglycan precursor. *Frontiers in Microbiology*, *9*, 1–10. https://doi.org/10.3389/fmicb.2018.00791

SUPPORTING INFORMATION

Additional supporting information may be found online in the Supporting Information section.

How to cite this article: Springstein BL, Arévalo S, Helbig AO, et al. A novel septal protein of multicellular heterocystous cyanobacteria is associated with the divisome. *Mol Microbiol*. 2020;113:1140–1154. https://doi.org/10.1111/mmi.14483